Efficient Luminescence from $CsPbBr_3$ nanoparticles embedded in Cs_4PbBr_6

Zhen Bao [1], Yu-Jui Tseng [1], Wenwu You[2], Wei Zheng[2], Xueyuan Chen[2], Sebastian Mahlik[3]*, Agata Lazarowska[3], Tadeusz Lesniewski[3], Marek Grinberg[3], Chonggeng Ma[4]*, Weihao Sun[5], Wuzong Zhou[5]*, Ru-Shi Liu[1,6,7]*, and J. Paul Attfield[8]**

[1]Department of Chemistry, National Taiwan University, Taipei, 106, Taiwan

[2]CAS Key Laboratory of Design and Assembly of Functional Nanostructures, and Fujian Key Laboratory of Nanomaterials, Fujian Institute of Research on the Structure of Matter, Chinese Academy of Sciences, Fuzhou, Fujian 350002, China

[3]Institute of Experimental Physics, Faculty of Mathematics, Physics and Informatics, University of Gdańsk, 80-308 Gdańsk, Poland

[4]CQUPT-BUL Innovation Institute, Chongqing University of Posts and Telecommunications, Chongqing 400065, China

[5]School of Chemistry, University of St Andrews, St Andrews KY16 9ST, United Kingdom

[6]Advanced Research Center of Green Materials Science and Technology, National Taiwan University, Taipei 106, Taiwan

[7]Department of Mechanical Engineering and Graduate Institute of Manufacturing Technology, National Taipei University of Technology, Taipei 106, Taiwan

[8]Centre for Science at Extreme Conditions and School of Chemistry, University of Edinburgh, King's Buildings, Mayfield Road, EH9 3JZ Edinburgh, United Kingdom

AUTHOR INFORMATION

Corresponding Authors

xchen@fjirsm.ac.cn (X. Chen)

s.mahlik@ug.edu.pl (S. Mahlik)

cgma.ustc@gmail.com (C. Ma)

wzhou@st-andrews.ac.uk (W. Zhou)

rsliu@ntu.edu.tw (R. S. Liu)

j.p.attfield@ed.ac.uk (J. P. Attfield)

ABSTRACT. Cs_4PbBr_6 is regarded as an outstanding luminescent material with good thermal stability and optical performance. However, the mechanism of green emission from Cs_4PbBr_6 has been controversial. Here we show that isolated $CsPbBr_3$ nanoparticles embedded within a Cs_4PbBr_6 matrix give rise to a “normal” green luminescence while superfluorescence at longer wavelengths is suppressed. High-resolution transmission electron microscopy shows that the embedded $CsPbBr_3$ nanoparticles are around 3.8 nm in diameter and are well-separated from each other, perhaps by a strain driven mechanism. This mechanism may enable other efficient luminescent composites to be developed by embedding optically active nanoparticles epitaxially within inert host lattices.

TOC GRAPHICS

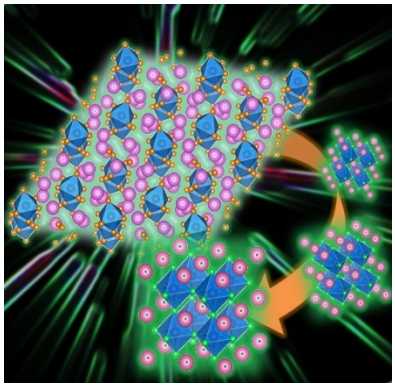

Keywords: $CsPbBr_3$; Cs_4PbBr_6; embedded; superfluorescence; nanocrystals

In recent years, lead halide perovskite materials have become regarded as a new generation of functional materials for solar cells, lasers, photodetectors and light-emitting diodes (LEDs).[1-6] Perovskite nanocrystals (NCs) are also considered to have great potential for backlight displays because of their excellent photoluminescence (PL) performance and quantum yield.[7-11] Although perovskite NCs have been successfully demonstrated in light-emitting devices, poor stability is the main limitation for commercial applications,[2, 12] and issues of thermal stability, photostability, water-resistance, and anion exchange need to be overcome.

One approach to solve these problems is to reduce the structural dimension.[13-17] In zero-dimensional perovskite-related Cs_4PbBr_6, strong green PL emission can be observed dependent on particle size.[14] The PL has been attributed to Br defects in the crystals,[18-21] but other studies[22] discovered $CsPbBr_3$ nanoparticles embedded in Cs_4PbBr_6 and proposed that the emission of green light comes from these rather than the Cs_4PbBr_6 host.[21, 23] However, further studies have suggested that the embedded $CsPbBr_3$ phase may tune an impurity mechanism for PL of Cs_4PbBr_6,[24] and the mechanism of green emission from Cs_4PbBr_6 remains under debate.[25] In this research, we have further explored the emission from Cs_4PbBr_6 and we have also tuned reagent ratios while synthesizing Cs_4PbBr_6 to explore the PL behavior and phase transform process, and we demonstrate that the embedded $CsPbBr_3$ nanoparticles are the origin of green emission in Cs_4PbBr_6 crystals.

Polycrystalline Cs_4PbBr_6 was synthesized by the antisolvent method with the Cs/Pb precursor ratio of 3.33, and $CsPbBr_3$ QDs for comparison were synthesized through a hot-injection method. Detailed processes are presented in the Methods section. Powder synchrotron X-ray diffraction (XRD) data in Figure. 1a shows that our Cs_4PbBr_6 crystals are single phase and the

previously reported rhombohedral structure (crystal open database; COD No.1538416) fits the data well with lattice parameters a = 13.72939(15) and c = 17.31874(25) Å (Table S1).

HRTEM, on the other hand, revealed many embedded dots (black spots in each particle) in the Cs_4PbBr_6 crystals, as shown in Figure. 1b. High-quality HRTEM images from this beam sensitive material have been recorded, showing the lattice fringes of the Cs_4PbBr_6 crystals as well as the embedded dots. As exhibited in Figure. 1c, the fringes "A" of the parent crystal have a *d*-spacing of 3.99 Å, corresponding to the (300) planes of the rhombohedral structure of Cs_4PbBr_6, while the fringes "B" in a dark dot have a *d*-spacing of 2.90 Å, which can be indexed to the (200) planes of the cubic $CsPbBr_3$ structure. The inset of Figure. 1c shows a size distribution of the embedded $CsPbBr_3$ nanoparticles based on a measurement of randomly selected 200 dots. Almost all these dots are smaller than 10 nm and their average size around 3.8 nm in diameter. The dark contrast of these embedded dots is mainly dominated by the mass contrast due to a relatively higher concentration of Pb in $CsPbBr_3$.

The [111] direction of the $CsPbBr_3$ nanoparticles observed by HRTEM is coincident with [001] of Cs_4PbBr_6 host crystals and the hexagonal symmetries of these phases match well in the (001) planes of Cs_4PbBr_6 with the [100] direction of Cs_4PbBr_6 parallel to [110] of $CsPbBr_3$. Consequently, the ideal inter-axes angle between the [100] of Cs_4PbBr_6 and the [100] of $CsPbBr_3$ is 65.9 degrees. The corresponding measured angle between the marked fringes in Figure. 1c is 63 degrees. The structural projection along the [001] zone axis of Cs_4PbBr_6 and the [111] axis of $CsPbBr_3$ (as shown in Figure. 1d) with the [100] direction of Cs_4PbBr_6 parallel to the [110] of $CsPbBr_3$ gives a good lattice match (a mismatch of +4.7% between $d_{100}(Cs_4PbBr_6)$ = 11.89 Å and $3d_{110}(CsPbBr_3)$ = 12.45 Å). Similarly in the [001] axis direction of Cs_4PbBr_6, the $d_{001}(Cs_4PbBr_6)$ = 17.32 Å has only a -2.1% mismatch to $5d_{111}(CsPbBr_3)$ = 16.945 Å. Although the lattice matching

is good, the slight mismatch will create a strain field in the host material that likely acts to limit the size of the $CsPbBr_3$ particles and keep them well separated, which is important to the optical properties as discussed below. Thus they can be embedded epitaxially into Cs_4PbBr_6 crystals.

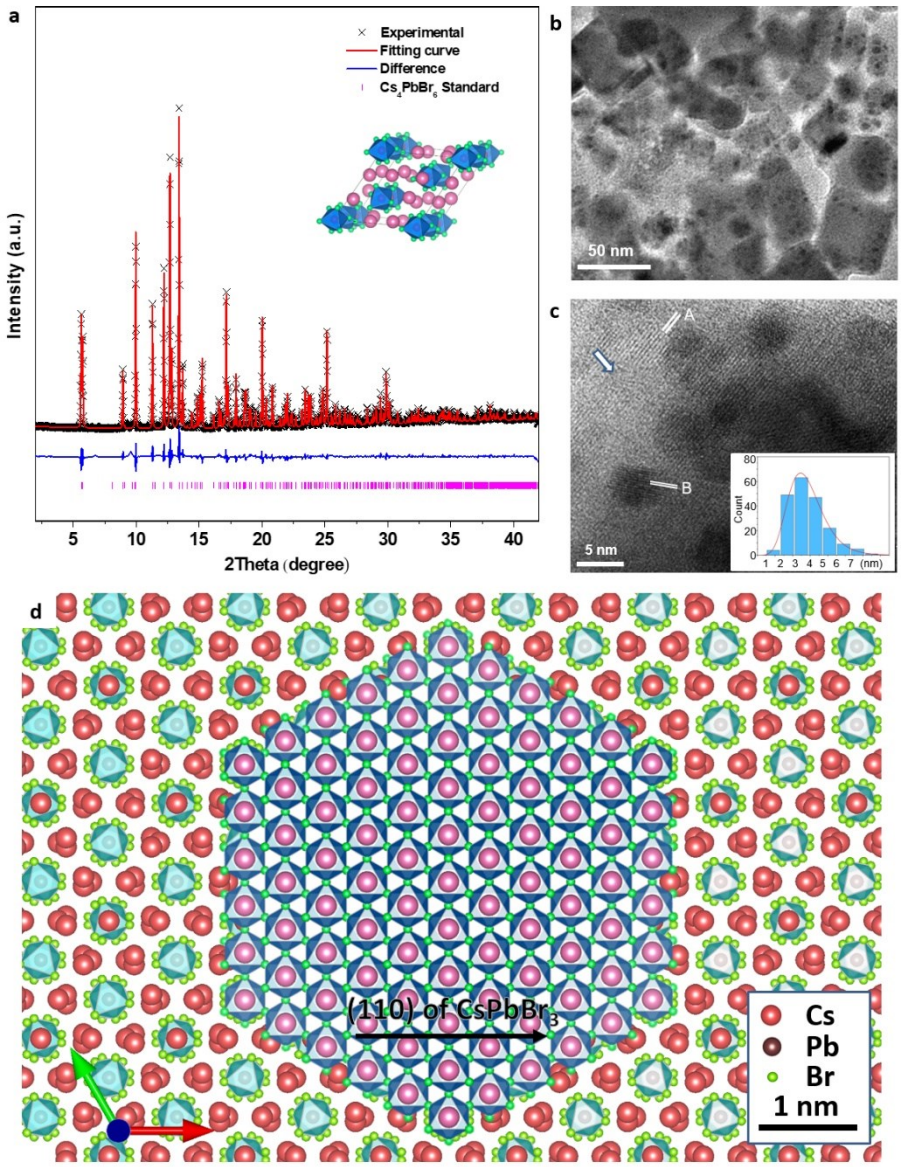

Figure 1. Structural characterization of the Cs_4PbBr_6 crystals. a, Refined synchrotron XRD (beamline energy 20 keV) pattern of the specimen. b, TEM image of Cs_4PbBr_6 crystals with embedded $CsPbBr_3$ crystals as dark dots. c, HRTEM image of a Cs_4PbBr_6 crystal with embedded $CsPbBr_3$ dots. The fringes marked A (d = 3.99 Å) are in the parent Cs_4PbBr_6 crystal region and

that marked B (d = 2.90 Å) in an embedded dot can be indexed to the $CsPbBr_3$ structure. The inset of (c) shows a size distribution of the embedded $CsPbBr_3$ dots, matching to a log-normal distribution curve. The arrow points to an area of slight crystal damage. d, Model showing how a $CsPbBr_3$ nanoparticle is embedded epitaxially within the Cs_4PbBr_6 host lattice, projected on the (001) plane of the latter.

To explore the optical behavior of Cs_4PbBr_6 crystals, we carried out temperature-dependent steady-state PL spectroscopy measurements (10-300 K). As shown in Figure. 2a, the crystals exhibited an intense green emission band in the spectral region from 490 nm to 550 nm upon above-bandgap excitation at 274 nm. When the temperature rose from 10 K to 300 K, the intensity of the emission band decreased greatly by a factor 6.7, along with an obvious blue-shift in peak wavelength from 530.5 nm to 520.0 nm. Such temperature-dependent PL behavior coincides very well with that of $CsPbBr_3$ quantum dots (QDs) previously reported,[26-27] suggesting that the green PL of Cs_4PbBr_6 crystals is dictated by the emission of $CsPbBr_3$ embedded in the lattice of Cs_4PbBr_6. Figure. 2b shows the temperature-dependent PL excitation spectra of Cs_4PbBr_6 crystals by monitoring the green emission at 524 nm, which displays broad excitation bands from 250 nm to 500 nm with "hole burning" at around 310 nm. The excitation band with the energy below 3.82 eV and above 4.13 eV are ascribed to the absorption of $CsPbBr_3$, while the temperature-dependent "hole burning" at 310 nm agrees well the localized exciton absorption of Cs_4PbBr_6 crystals.[28] This can be further verified by the temperature-dependent PL emission spectra of Cs_4PbBr_6 crystals upon excitation at 310 nm, as shown in Figure. 2c. As the temperature fell below 200 K, the green emission of $CsPbBr_3$ was detected along with an ultra-violet emission with a central wavelength at 375 nm. The emission band at 375 nm can be assigned to the $^3P_0 \rightarrow {}^1S_0$ transition of Pb^{2+} ion in isolated $[PbBr_6]^{4-}$ octahedra.[29-31] Meanwhile, it was found that both the $CsPbBr_3$ and Pb^{2+}

emissions weakened significantly with the temperature rise and nearly vanished when the temperature was higher than 200 K, due to the increased thermal quenching at higher temperatures. 10 K PL excitation spectrum of the crystals by monitoring the Pb^{2+} emission at 375 nm shows a strong excitation band around 310 nm, ascribed to the $^1S_0 \rightarrow {}^3P_1$ transition of Pb^{2+} ion in isolated $[PbBr_6]^{4-}$ octahedra in Cs_4PbBr_6 (Figure. 2d). In summary, the temperature-dependent PL evolution for the green emission of Cs_4PbBr_6 crystals is very similar to that of $CsPbBr_3$ QDs.

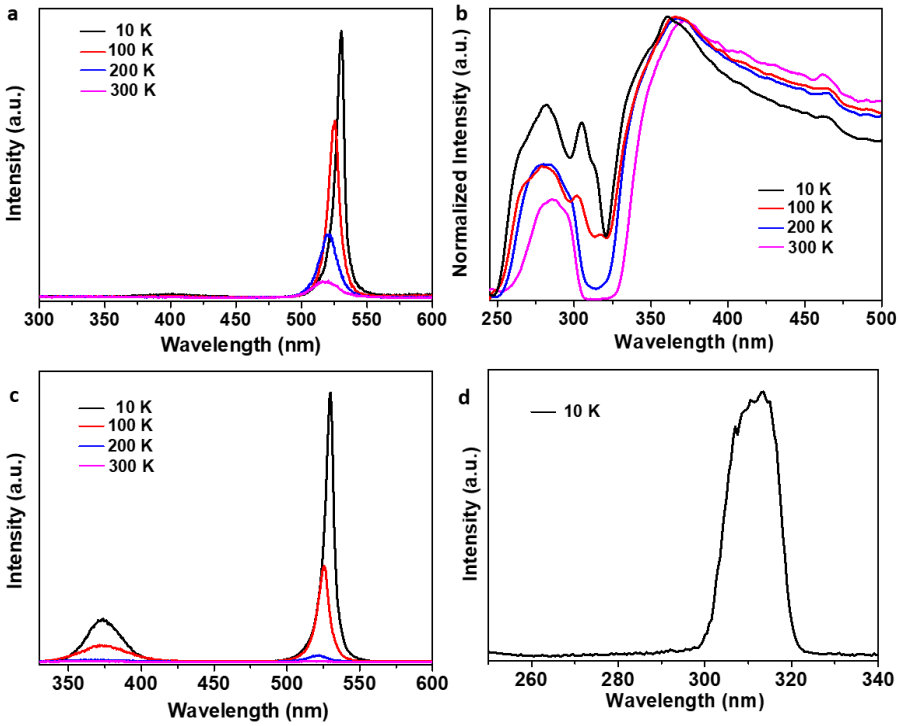

Figure 2. Photoluminescence of the Cs_4PbBr_6 sample. a, Temperature-dependent PL emission spectra of Cs_4PbBr_6 upon excitation at 274 nm in the temperature range of 10–300 K. b, Normalized PL excitation spectra of Cs_4PbBr_6 as a function of temperature by monitoring the $CsPbBr_3$ emission at 524 nm. c, Temperature-dependent PL emission spectra of Cs_4PbBr_6 upon excitation at 310 nm in the temperature range of 10–300 K. d, 10 K PL excitation spectrum of Cs_4PbBr_6 by monitoring the Pb^{2+} emission at 375 nm.

To further examine the type of luminescence centers in the green-emitting Cs_4PbBr_6 material, the time-resolved emission spectra of Cs_4PbBr_6 crystals and dried $CsPbBr_3$ QD powders (for comparison) were compared in the temperature range of 10-300 K. Figure. 3 presents time-resolved emission spectra (streak images) of Cs_4PbBr_6 crystals (Figures. 3a, b, c) and $CsPbBr_3$ QDs (Figures. 3d, e, f) obtained at a time range of 1 ns. The room temperature streak images of both Cs_4PbBr_6 crystals and $CsPbBr_3$ QDs systems show an emission band located around the same central wavelength (520 nm), however with different FWHM (~10 nm for Cs_4PbBr_6 crystals and ~30 nm for $CsPbBr_3$ QDs). As the temperature decreases the FWHM of both systems decreases, most significantly for $CsPbBr_3$ QDs which is accompanied by a shift of the emission center towards red (green curves in Figures. 3d, e, f). $CsPbBr_3$ QDs at the temperature lower than 250 K exhibit an additional type of luminescence, possessing emission wavelength slightly shifted towards the red (red curves in Figures. 3d, e). Under pulsed excitation, the intensity of the additional luminescence is much greater than the regular emission and the decay time of the luminescence is at least an order of magnitude shorter than the regular luminescence of $CsPbBr_3$ QDs. The precise determination of the decay time was not possible due to the finite duration of the excitation pulse (FWHM ~30 ps, see the pink curve in Figures. 3 a-f).

We interpret the additional luminescence as superfluorescence[28] – luminescence due to the collective emission of multiple QDs located close to each other (at distances below the wavelength of the emitted light) so light emission from a QD can induce synchronous emission from nearby QDs. As a result, the QDs emit light collectively due to induced emission, with a much greater radiative rate, which corresponds to a much shorter decay time (of the order of picoseconds). The streak images of low-temperature emission in $CsPbBr_3$ QDs (Figure 3d, e) show intense, short-time superfluorescence from QDs remaining in proximity (coupled QDs) as well as residual

luminescence from the QDs that are too far from other QDs to emit collectively (uncoupled QDs). The Cs_4PbBr_6 sample does not exhibit superfluorescence at any temperature which indicated that the QDs embedded in the Cs_4PbBr_6 matrix are too far apart to exhibit coupling. In contrast, the free $CsPbBr_3$ QDs tend to agglomerate easily leading to coupling and superfluorescence. High-pressure studies also confirmed that the green PL of Cs_4PbBr_6 originates from the emission of $CsPbBr_3$ embedded in the lattice of Cs_4PbBr_6 (shown in Supplementary Information). Hence, this study demonstrates that embedded $CsPbBr_3$ nanoparticles in Cs_4PbBr_6 show different emission properties to aggregates of free $CsPbBr_3$ QDs.

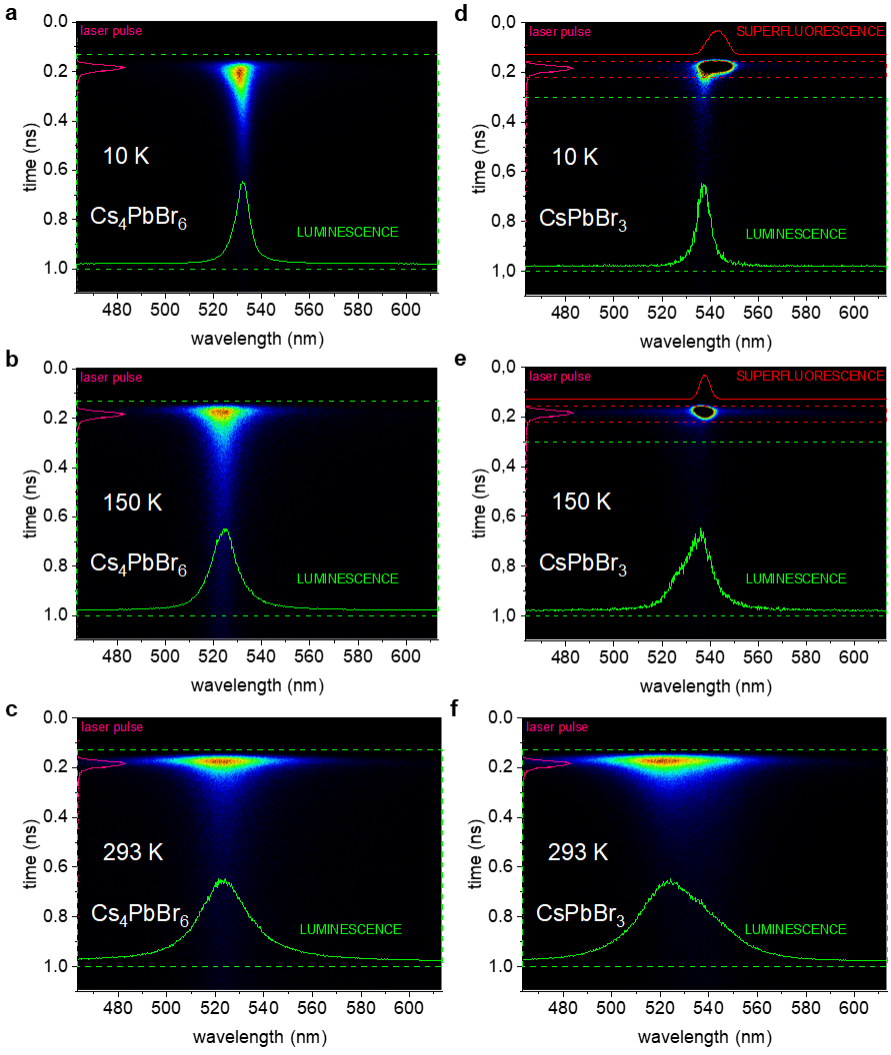

Figure 3. Time-resolved emission spectra (streak images) at a time range of 1 ns. Cs_4PbBr_6 sample at 10K (**a**), 150 K (**b**), 293 K (**c**). $CsPbBr_3$ QDs at 10K (**d**), 150 K (**e**), 293 K (**f**). The green curve presents an integrated emission spectrum of light emitted in the time interval denoted by the green dashed lines. The red curve denotes the integrated emission spectrum of superfluorescence. The pink curve denotes the temporal shape of the excitation laser pulse.

It is important to find how synthesis conditions affect the formation of embedded $CsPbBr_3$ in Cs_4PbBr_6. Hence we have synthesized a series of materials with the ratio of Cs/Pb reactants varied in the range from 1 to 4.5 using the same synthesis procedure as for the original Cs_4PbBr_6 sample. From the XRD patterns, as shown in Figure. 4a, polycrystalline Cs_4PbBr_6 remains the only phase observed by XRD with the Cs/Pb ratio between 4.5 and 2.5. Peaks from the secondary phase of $CsPbBr_3$ begin to emerge at a Cs/Pb ratio of 2.25, and increase in intensity as the Cs/Pb ratio decreases to 1. Correspondingly, the external quantum efficiency (EQE) of the samples rises smoothly up to 28.4% as the Cs/Pb ratio decreased from 4.5 to 2.5, as the concentration of embedded $CsPbBr_3$ nanoparticles increases with falling Cs/Pb ratio, (Figure. 4b) but sharply decreases from 28.4% to 14.7% when the Cs/Pb precursor ratio reached 2.25, where secondary $CsPbBr_3$ phase starts to emerge (Figure. 4c). $CsPbBr_3$ has high photoluminescence if particle size is smaller than ~10 nm, but for Cs/Pb ratios below 2.5, the unconstrained secondary phase particles aggregate to larger sizes leading to their appearence in XRD patterns and the observed drop in overall EQE. These results thus confirm that the high-quality green PL emission of the Cs_4PbBr_6 is from embedded $CsPbBr_3$ nanoparticles, while any secondary $CsPbBr_3$ phase luminescences with a much lower EQE.

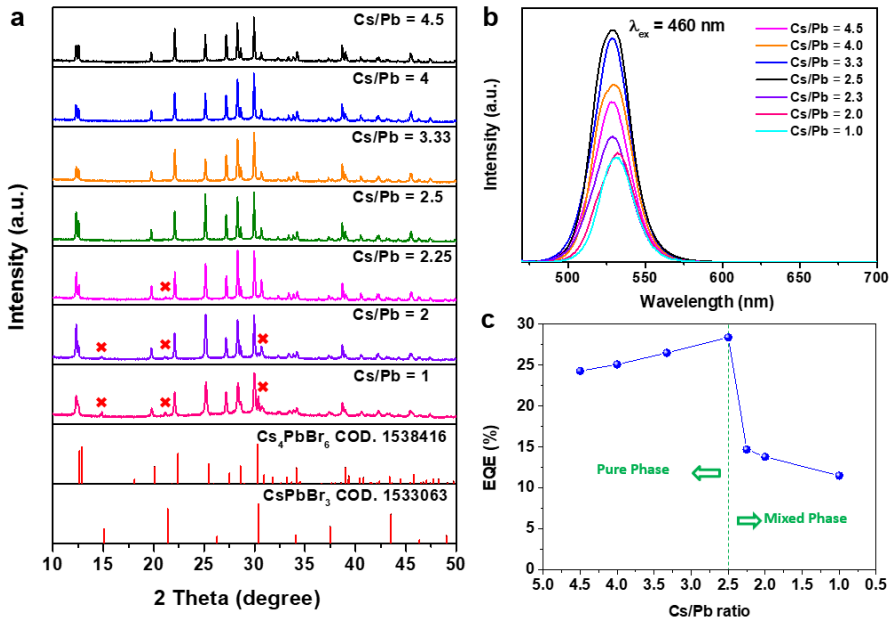

Figure 4. Properties of Cs_4PbBr_6 samples when tuning the Cs/Pb precursor ratio. a, XRD patterns, b, Normalized PL emission spectra, and c, EQE, of Cs_4PbBr_6 samples synthesized with different Cs/Pb precursor ratios, showing single and mixed phase regions as observed by XRD.

In summary, our results demonstrate that epitaxially embedded $CsPbBr_3$ nanoparticles are responsible for the efficient green emission from Cs_4PbBr_6 crystals. $CsPbBr_3$ impurity phase may also be present if samples are synthesized with a Cs/Pb precursor ratio lower than 2.5, but these have lower emission intensity. Our study shows that the properties of optically active nanoparticles are significantly altered by embedding them in a suitable inert host lattice, and this mechanism may enable further new efficient luminescent composites to be developed.

ASSOCIATED CONTENT

Supporting Information. The Supporting Information is available free of charge on the ACS Publications website at DOI: 10.1021/acsenergylett.XXXXXXX.

Complete experimental section, optical properties, further temperature-dependent PL properties, and pressure-dependent PL properties.

AUTHOR INFORMATION

Corresponding Authors

xchen@fjirsm.ac.cn (X. Chen)

s.mahlik@ug.edu.pl (S. Mahlik)

cgma.ustc@gmail.com (C. Ma)

wzhou@st-andrews.ac.uk (W. Zhou)

rsliu@ntu.edu.tw (R. S. Liu)

j.p.attfield@ed.ac.uk (J. P. Attfield)

Notes

The authors declare no competing financial interest.

ACKNOWLEDGMENT

This work was financially supported by the "Advanced Research Center of Green Materials Science and Technology" from The Featured Area Research Center Program within the framework of the Higher Education Sprout Project by the Ministry of Education (107L9006) and the Ministry of Science and Technology in Taiwan (MOST 107-2113-M-002-008-MY3, MOST 107-2923-M-002-004-MY3 and MOST 107-3017-F-002-001), the National Centre for Research and Development Poland Grant (No. PL-TW/V/1/2018), the Strategic Priority Research Program of the Chinese Academy of Sciences (XDB20000000), the CAS/SAFEA International Partnership Program for Creative Research Teams, and the NSFC (nos. U1805252 and 11774345). J.P.A. acknowledges financial support from EPSRC, UK.

REFERENCES

(1) Stranks, S. D.; Snaith, H. J. Metal-Halide Perovskites for Photovoltaic and Light-Emitting Devices. *Nat. Nanotechnol.* **2015,** *10*, 391–402.

(2) Li, J.; Xu, L.; Wang, T.; Song, J.; Chen, J.; Xue, J.; Dong, Y.; Cai, B.; Shan, Q.; Han, B.; Zeng, H. 50-Fold EQE Improvement up to 6.27% of Solution-Processed All-Inorganic Perovskite $CsPbBr_3$ QLEDs via Surface Ligand Density Control. *Adv. Mater.* **2017,** *29*, 1603885.

(3) Sutherland, B. R.; Sargent, E. H. Perovskite Photonic Sources. *Nat. Photonics* **2016,** *10*, 295–302.

(4) Forgács, D.; Gil-Escrig, L.; Pérez-Del-Rey, D.; Momblona, C.; Werner, J.; Niesen, B.; Ballif, C.; Sessolo, M.; Bolink, H. J. Efficient Monolithic Perovskite/Perovskite Tandem Solar Cells. *Adv. Energy Mater.* **2017,** *7*, 1602121.

(5) Wang, Y.; Li, X.; Song, J.; Xiao, L.; Zeng, H.; Sun, H. All-Inorganic Colloidal Perovskite Quantum Dots: A New Class of Lasing Materials with Favorable Characteristics. *Adv. Mater.* **2015,** *27*, 7101−7108.

(6) Song, J.; Xu, L.; Li, J.; Xue, J.; Dong, Y.; Li, X.; Zeng, H. Monolayer and Few-Layer All-Inorganic Perovskites as a New Family of Two-Dimensional Semiconductors for Printable Optoelectronic Devices. *Adv. Mater.* **2016,** *28*, 4861–4869.

(7) Zhang, F.; Zhong, H.; Chen, C.; Wu, X.-g.; Hu, X.; Huang, H.; Han, J.; Zou, B.; Dong, Y. Brightly Luminescent and Color-Tunable Colloidal $CH_3NH_3PbX_3$ (X = Br, I, Cl) Quantum Dots: Potential Alternatives For Display Technology. *ACS Nano* **2015,** *9*, 4533–4542.

(8) Protesescu, L.; Yakunin, S.; Bodnarchuk, M. I.; Krieg, F.; Caputo, R.; Hendon, C. H.; Yang, R. X.; Walsh, A.; Kovalenko, M. V. Nanocrystals of cesium lead halide perovskites (CsPbX3, X= Cl, Br, and I): novel optoelectronic materials showing bright emission with wide color gamut. *Nano Lett.* **2015,** *15*, 3692-3696.

(9) Li, Z.; Kong, L.; Huang, S.; Li, L. Highly Luminescent and Ultrastable $CsPbBr_3$ Perovskite Quantum Dots Incorporated into A Silica/Alumina Monolith. *Angew. Chem.* **2017,** *129*, 8246–8250.

(10) Wang, H. C.; Bao, Z.; Tsai, H. Y.; Tang, A. C.; Liu, R. S. Perovskite Quantum Dots and Their Application in Light‐Emitting Diodes. *Small* **2018,** *14*, 1702433.

(11) Wang, H. C.; Wang, W.; Tang, A. C.; Tsai, H. Y.; Bao, Z.; Ihara, T.; Yarita, N.; Tahara, H.; Kanemitsu, Y.; Chen, S. High‐Performance $CsPb_{1-x}Sn_xBr_3$ Perovskite Quantum Dots for Light‐Emitting Diodes. *Angew. Chem.* **2017,** *129*, 13838–13842.

(12) Huang, H.; Zhao, F.; Liu, L.; Zhang, F.; Wu, X.-g.; Shi, L.; Zou, B.; Pei, Q.; Zhong, H. Emulsion Synthesis of Size-Tunable $CH_3NH_3PbBr_3$ Quantum Dots: An Alternative Route Toward Efficient Light-Emitting Diodes. *ACS Appl. Mater. Interfaces* **2015,** *7*, 28128-28133.

(13) Kondo, S.; Amaya, K.; Saito, T. Localized Optical Absorption in Cs_4PbBr_6. *J. Phys.: Condens. Matter* **2002,** *14*, 2093.

(14) Saidaminov, M. I.; Almutlaq, J.; Sarmah, S.; Dursun, I.; Zhumekenov, A. A.; Begum, R.; Pan, J.; Cho, N.; Mohammed, O. F.; Bakr, O. M. Pure Cs_4PbBr_6: Highly Luminescent Zero-Dimensional Perovskite Solids. *ACS Energy Lett.* **2016,** *1*, 840–845.

(15) Saparov, B.; Mitzi, D. B. Organic–Inorganic Perovskites: Structural Versatility for Functional Materials Design. *Chem. Rev.* **2016,** *116*, 4558–4596.

(16) Sum, T. C.; Mathews, N. Advancements in Perovskite Solar Cells: Photophysics Behind the Photovoltaics. *Energy Environ. Sci.* **2014,** *7*, 2518–2534.

(17) Velázquez, M.; Ferrier, A.; Péchev, S.; Gravereau, P.; Chaminade, J. P.; Portier, X.; Moncorgé, R. Growth and characterization of pure and Pr^{3+}-doped Cs_4PbBr_6 crystals. *J. Cryst. Growth* **2008,** *310*, 5458–5463.

(18) De Bastiani, M.; Dursun, I.; Zhang, Y.; Alshankiti, B. A.; Miao, X.-H.; Yin, J.; Yengel, E.; Alarousu, E.; Turedi, B.; Almutlaq, J. M.; Saidaminov, M. I.; Mitra, S.; Gereige, I.; Alsaggaf, A.; Zhu, Y.; Han, Y.; Roqan, I. S.; Bredas, J.-L.; Mohammed, O. F.; Bakr, O. M. Inside Perovskites: Quantum Luminescence from Bulk Cs_4PbBr_6 Single Crystals. *Chem. Mater.* **2017,** *29*, 7108–7113.

(19) Ling, Y.; Tan, L.; Wang, X.; Zhou, Y.; Xin, Y.; Ma, B.; Hanson, K.; Gao, H. Composite Perovskites of Cesium Lead Bromide for Optimized Photoluminescence. *J. Phys. Chem. Lett* **2017,** *8*, 3266–3271.

(20) Seth, S.; Samanta, A. Fluorescent Phase-Pure Zero-Dimensional Perovskite-Related Cs_4PbBr_6 Microdisks: Synthesis and Single-Particle Imaging Study. *J. Phys. Chem. Lett* **2017,** *8*, 4461–4467.

(21) Xu, J.; Huang, W.; Li, P.; Onken, D. R.; Dun, C.; Guo, Y.; Ucer, K. B.; Lu, C.; Wang, H.; Geyer, S. M. Imbedded Nanocrystals of $CsPbBr_3$ in Cs_4PbBr_6: Kinetics, Enhanced Oscillator Strength, and Application in Light‐Emitting Diodes. *Adv. Mater.* **2017,** *29*, 1703703.

(22) Quan, L. N.; Quintero‐Bermudez, R.; Voznyy, O.; Walters, G.; Jain, A.; Fan, J. Z.; Zheng, X.; Yang, Z.; Sargent, E. H. Highly Emissive Green Perovskite Nanocrystals in A Solid State Crystalline Matrix. *Adv. Mater.* **2017,** *29*, 1605945.

(23) Akkerman, Q. A.; Park, S.; Radicchi, E.; Nunzi, F.; Mosconi, E.; De Angelis, F.; Brescia, R.; Rastogi, P.; Prato, M.; Manna, L. Nearly Monodisperse Insulator Cs_4PbX_6 (X = Cl, Br, I) Nanocrystals, Their Mixed Halide Compositions, and Their Transformation into $CsPbX_3$ Nanocrystals. *Nano Lett.* **2017,** *17*, 1924–1930.

(24) Chen, X.; Zhang, F.; Ge, Y.; Shi, L.; Huang, S.; Tang, J.; Lv, Z.; Zhang, L.; Zou, B.; Zhong, H. Centimeter‐Sized Cs_4PbBr_6 Crystals with Embedded $CsPbBr_3$ Nanocrystals Showing Superior Photoluminescence: Nonstoichiometry Induced Transformation and Light‐Emitting Applications. *Adv. Funct. Mater.* **2018,** *28*, 1706567.

(25) Yin, J.; Yang, H.; Song, K.; El-Zohry, A. M.; Han, Y.; Bakr, O. M.; Brédas, J.-L.; Mohammed, O. F. Point Defects and Green Emission in Zero-Dimensional Perovskites. *J. Phys. Chem. Lett* **2018,** *9*, 5490–5495.

(26) Diroll, B. T.; Zhou, H.; Schaller, R. D. Low‐Temperature Absorption, Photoluminescence, and Lifetime of $CsPbX_3$ (X = Cl, Br, I) Nanocrystals. *Adv. Funct. Mater.* **2018,** *28*, 1800945.

(27) Balena, A.; Perulli, A.; Fernandez, M.; De Giorgi, M. L.; Nedelcu, G.; Kovalenko, M. V.; Anni, M. Temperature Dependence of the Amplified Spontaneous Emission from $CsPbBr_3$ Nanocrystal Thin Films. *J. Phys. Chem. C* **2018,** *122*, 5813–5819.

(28) Rainò, G.; Becker, M. A.; Bodnarchuk, M. I.; Mahrt, R. F.; Kovalenko, M. V.; Stöferle, T. Superfluorescence from Lead Halide Perovskite Quantum Dot Superlattices. *Nature* **2018,** *563*, 671-675.

(29) Cheetham, A. K.; Wilkinson, A. P. Synchrotron X‐ray and Neutron Diffraction Studies in Solid‐State Chemistry. *Angew. Chem. Int. Ed.* **1992,** *31*, 1557–1570.

(30) Babin, V.; Oskam, K. D.; Vergeer, P.; Meijerink, A. The Role of Pb^{2+} as A Sensitizer for Gd^{3+}–Eu^{3+} Downconversion Couple in Fluorides. *Radiation measurements* **2004,** *38*, 767–770.

(31) Sun, Q.; Wang, J.; Shi, J. Prediction and Assignment of Site Occupation And Energy Levels for Pb^{2+} Ions in Crystal Hosts. *J. Solid State Chem.* **2010,** *183*, 1174–1179.